IEEE Access
Multidisciplinary | Rapid Review | Open Access Journal

Received February 28, 2018, accepted April 2, 2018, date of publication April 17, 2018, date of current version May 24, 2018.

Digital Object Identifier 10.1109/ACCESS.2018.2827921

Position Accuracy of Joint Time-Delay and Channel Estimators in LTE Networks

JOSÉ A. DEL PERAL-ROSADO[1], (Member, IEEE), JOSÉ A. LÓPEZ-SALCEDO[1], (Senior Member, IEEE), FRANCESCA ZANIER[2], AND GONZALO SECO-GRANADOS[1], (Senior Member, IEEE)

[1]Department of Telecommunications and Systems Engineering, Universitat Autònoma de Barcelona, 08193 Bellaterra, Spain
[2]European Space Research and Technology Centre, European Space Agency, 2201 AZ Noordwijk, The Netherlands

Corresponding author: José A. del Peral-Rosado (joseantonio.delperal@uab.cat)

This work was supported in part by the European Space Agency under NPI program under Grant 4000110780/14/NL/AK and in part by the Spanish Ministry of Science and Innovation project under Grant TEC2014-53656-R and Grant TEC2017-89925-R.

ABSTRACT Future mobile applications are expected to demand high accuracy positioning from cellular networks. However, most time-delay estimators used for cellular trilateration ignore the multipath channel, resulting in a poor positioning performance. This paper investigates the use of advanced joint time-delay and channel estimation techniques for Long Term Evolution (LTE) mobile localization, as a predecessor of fifth generation (5G) technologies. This is especially relevant for sub-6 GHz bands, where the bandwidth and the dedicated positioning resources are limited. Thus, joint maximum likelihood (JML) estimators are presented in order to reach the achievable ranging accuracy, which is first assessed with the derivation of their Cramér-Rao bound (CRB). Simulation and laboratory experiments are then used to obtain an estimation of their achievable positioning performance. Periodic-tap JML estimators are shown to achieve the best position accuracy with respect to state-of-the-art threshold-based and super-resolution techniques, due to their robustness against multipath overlapping and noise effects for reduced bandwidths. A robust position accuracy of around 10 meters for a 10-MHz system bandwidth can be achieved with periodic-tap JML estimators in challenging urban environments.

INDEX TERMS LTE localization, time-delay estimation, channel estimation, position accuracy.

I. INTRODUCTION

There is a significant interest on cellular radio localization from the standardization bodies, the industry and the research community [1], due to the provision of the mobile location for emergency services [2], the benefits of location-aware communications [3], and the potential exploitation of location-based services (LCS). Furthermore, future mobile applications are expected to require a high accuracy and reliability in cellular localization [4], such as autonomous vehicles, float management, asset tracking, or mission-critical applications. Nowadays, the mobile location information is typically obtained from Global Navigation Satellite Systems (GNSS), which have global coverage and good performance in perfect clear sky, but suffer from limited satellite visibility in urban canyons and indoors. An attractive alternative is the use of the cellular network itself, by means of proximity, trilateration or fingerprinting techniques. The current Long Term Evolution (LTE) standard already dedicates network resources and methods for positioning in [5] and [6], such as the positioning reference signal (PRS), the PRS muting and the LTE positioning protocol (LPP). In addition, indoor positioning enhancements have been studied within the standardization process in [7], by targeting a horizontal position accuracy of 50 meters for E911 emergency services [2]. Moreover, there is an increasing interest on the exploitation of high accuracy positioning in LTE, such as in [8], as a predecessor of future fifth generation (5G) networks.

The most accurate cellular-based location method in LTE is based on time-difference of arrival (TDoA) measurements. However, the TDoA-based position accuracy is mainly limited due to dense multipath in urban environments. Experimental field measurements in [9] already show this harsh environment, where a median position accuracy of 20 meters is only obtained for a 20-MHz PRS. In addition, TDoA localization needs a tight network synchronization, which implies an extra implementation cost. All these considerations have led to a limited adoption of TDoA-based localization in

commercial LTE networks [10]. In this context, the LTE transmissions can only be used as signals of opportunity for positioning, as it is assessed with field measurements of vehicular scenarios from two different setups in [11] and [12]. However, the positioning performance and applicability of these opportunistic techniques are limited by the hearibility problem of neighbour base stations (BSs), the estimation of the network synchronization and the multipath channel. Thus, multipath countermeasures are required to achieve high accuracy positioning with ranging-based techniques, by taking advantage of the LTE interference-avoidance schemes and dedicated positioning resources.

There are two main and complementary strategies for multipath mitigation, which are based on the position calculation and the time-delay estimation (TDE). At the position level, a survey of localization methods for line-of-sight (LoS) and non-LoS (NLoS) conditions is provided in [13], where most of the robust algorithms are aimed at suppressing outlier estimations. In addition, TDoA error models can be used as prior knowledge in the localization algorithm. In [14], indoor field measurements are first used to characterize the TDoA error, and this model is then applied in a particle filter. Theoretical expressions are presented in [15] to compensate the expected TDoA bias. Skew-t distributed ranging errors are modelled with LTE laboratory measurements in [16], and the resulting skew-t parameters are considered in the statistical trilateration to mitigate the multipath effect for a low signal bandwidth. However, the main drawback of these techniques is the prior knowledge required on the TDoA error distribution. At the TDE level, threshold-based time-delay estimators have been widely adopted for multipath mitigation due to their low complexity, as reviewed in [17] and [18]. However, they have a relatively poor positioning performance even with a 10-MHz LTE bandwidth, as in [19]. Advanced algorithms are based on the joint time-delay and channel estimation. Super-resolution TDE techniques have been proposed, such as in [20], and their ranging performance bounds are studied over multipath channels in [21]. Joint maximum likelihood (JML) time-delay estimators are presented in [22], in order to assess the achievable LTE ranging performance in standard multipath scenarios. However, to the best of the authors' knowledge, there has not been a thorough study of the positioning performance for different types of time-delay estimators in cellular localization. In addition, these multipath countermeasures should require more advanced estimation techniques than conventional estimators, in order to achieve accurate positioning in urban scenarios.

The objective of this paper is to assess the LTE ranging capabilities as a testbench for future 5G technologies. The future 5G standard is expected to inherit or adopt similar physical-layer features of LTE, such as the multicarrier modulation. Furthermore, sub-6 GHz bands are expected to have limited resources in terms of signal bandwidth and positioning pilots. Thus, the achievable positioning performance of joint time-delay and channel estimators is assessed with LTE pilot signals. Three novel contributions are provided in this paper. First, fundamental lower bounds are derived for each type of joint time-delay and channel estimation. Second, the performance limits of existing estimators are evaluated for representative multipath models. Third, laboratory experiments are conducted to assess the achievable position accuracy in LTE networks with practical impairments.

The outline of the paper is as follows. First, the fundamentals of LTE positioning are described in Section II. The multicarrier signal and channel estimation models are defined in Section III. The corresponding Cramér-Rao bound (CRB) of these estimation models is derived in Section IV. The joint time-delay and channel estimation is introduced in Section V. Then, the achievable ranging accuracy is assessed with simulations in Section VI. The ranging and positioning performance is evaluated with laboratory measurements in Section VII. Finally, the conclusions and future work are drawn in Section VIII.

II. LTE POSITIONING

The main positioning capabilities of the LTE technology are described in this section, by including the last updates of the LTE-Advanced Pro standard in Release 13. The physical layer and the positioning methods are first introduced. Then, the focus is on LTE ranging-based localization, where the main challenges and fundamental limits are defined.

A. PHYSICAL LAYER

The physical layer of cellular systems is defined by the downlink or uplink channels, depending on whether the signal transmission is from BS to mobile device or from the mobile device to BS, respectively. In LTE, orthogonal frequency division multiple access (OFDMA) is used for the downlink access, and single carrier FDMA (SC-FDMA) for the uplink access. Both access modes are based on OFDM multicarrier modulation. These transmission modes contain reference signals to aid the demodulation of the data signals. These reference signals or pilots can also be used to perform ranging measurements, such as the synchronization signals, the cell-specific reference signal (CRS) and the PRS in the downlink, and the sounding reference signal (SRS) in the uplink. Indeed, the PRS is a dedicated pilot signal for positioning, which is designed to avoid inter-cell interference and multipath. Although the propagation channel is the same for both downlink and uplink multicarrier signals, the transmission power and the interference mitigation mechanisms are different. This paper considers only the downlink physical channel, but it is also applicable in the uplink case for similar signal power conditions without interference.

The resource allocation of the LTE downlink is defined in a time-frequency grid formed by OFDM symbols and subcarriers [5]. The subcarrier spacing F_{sc} is equal to 15 kHz, which results in a symbol period of $T = 1/F_{\text{sc}} = 66.67\ \mu$s. The minimum resource allocation is called resource block (RB), which consists of 12 subcarriers and 7 OFDM symbols for the normal configuration mode. A cyclic prefix (CP) is added before every OFDM symbol, in order to avoid

TABLE 1. Standard LTE positioning methods [6].

Positioning method	Type of method	Stand-alone or network-based	Expected hor. accuracy
A-GNSS	Trilateration	Both	Very high
E-CID	Proximity	Network-based	Low
OTDoA	Trilateration	Network-based	High
UTDoA	Trilateration	Network-based	High
Barometer	Sensor	Both	–
WLAN	Fingerprinting	Both	Medium
Bluetooth	Fingerprinting	Both	Medium
TBS	Trilateration	Both	High
Hybrid	Mixed	Both	Very high

inter-symbol interference. The resource allocation is repeated every radio frame of 10 ms, which is divided in ten subframes of 1 ms (formed by 14 OFDM symbols). The signal bandwidth of the CRS and PRS is defined between the minimum and maximum frequency of the N_{RS} pilot subcarriers, i.e., $B_{\mathrm{RS}} = N_{\mathrm{RS}} \cdot F_{\mathrm{sc}} = (12 \cdot N_{\mathrm{RB}} - 4) \cdot F_{\mathrm{sc}}$, where N_{RB} is the number of RBs. Since $N_{\mathrm{RB}} = \{6, 15, 25, 50, 75, 100\}$ RBs in LTE, the resulting signal bandwidth is $B_{\mathrm{RS}} = \{1.02, 2.64, 4.44, 8.94, 13.44, 17.94\}$ MHz. The LTE system bandwidth is defined by the total number of active subcarriers and the guard bands, which is $B_{\mathrm{LTE}} = \{1.4, 3, 5, 10, 15, 20\}$ MHz. By using carrier aggregation (CA), multiple LTE bands can be combined up to a system bandwidth of 100 MHz.

B. POSITIONING METHODS

The LTE technology has supported mobile positioning since Release 9 of the standard, and it has adopted new methods in the subsequent releases [1]. The positioning methods specified up to Release 13 of TS 36.305 [6] are assisted GNSS (A-GNSS), enhanced cell ID (E-CID), observed TDoA (OTDoA), uplink TDoA (UTDoA), barometric sensors, WLAN positioning, Bluetooth positioning, terrestrial beacon system (TBS) positioning, and hybrid positioning. A summary of these methods is provided in Table 1. The most promising LTE positioning methods in terms of horizontal accuracy are those based on ranging measurements, such as A-GNSS, OTDoA, UTDoA or TBS. However, with the exception of A-GNSS, these methods require additional infrastructure or mobile device modifications that have limited their deployment. In addition, network control on the mobile position calculation poses important privacy issues. Still, ranging-based localization is foreseen to be a pivotal functionality for high positioning accuracy applications in 5G. It is for this reason that determining the achievable localization accuracy in LTE (i.e., based on OTDoA) becomes the cornerstone for understanding the needs of future 5G networks.

C. OTDOA-BASED LOCALIZATION

The OTDoA method is studied herein, as an example of ranging-based LTE localization. This method is based on the trilateration of downlink ranging measurements in order to calculate the mobile position. For the sake of simplicity, let us define the horizontal distance or range between the i-th BS and the mobile as

$$d_i = c \cdot \tau_i = \|\mathbf{x}_i - \mathbf{x}\|, \tag{1}$$

where c is the speed of light, τ_i is the propagation time delay, $\|\cdot\|$ is the Euclidean distance, $\mathbf{x}_i = [x_i, y_i]^{\mathrm{T}}$ is the known BS position, and $\mathbf{x} = [x, y]^{\mathrm{T}}$ is the unknown mobile position. The measured distance or observed pseudorange is

$$\rho_i = c \cdot \hat{\tau}_i = \|\mathbf{x}_i - \mathbf{x}\| + c \cdot \delta t + e_i, \tag{2}$$

where $\hat{\tau}_i$ is the time-delay estimate, δt is the unknown clock offset of the mobile with respect to the reference time, and e_i is the pseudorange error. This error can be defined as

$$e_i = c \cdot \delta t_i + M_i + I_i + w_i, \tag{3}$$

where δt_i is the clock offset of the i-th BS with respect to the reference time, M_i is the multipath contribution, I_i is the interference contribution, and w_i is the noise contribution. In view of the pseudorange signal model, four main challenges can be identified in the mobile localization problem:

1) INFRASTRUCTURE

Tight network synchronization is required to achieve accurate localization with trilateration techniques. For instance, a clock time difference between BSs of 100 ns is equivalent to a position error of 30 meters. This implies that the BS clock offset has to be accurately calibrated. In addition, the location of the BSs has to be precisely known in order to not introduce further biases in the position calculation. However this information is only provided to the LTE location server within the network.

2) INTERFERENCE

Due to the limited time and frequency resources, LTE reuses the same frequency band between different BSs. For instance, the macro cell coverage is complemented in hotspots with small cells, which may have the same cell identity (CID), resulting in inter-cell interference. This interference is mitigated by using the PRS, which has a frequency reuse factor equal to six, and the PRS muting mechanism, which coordinates the PRS transmission among the different BSs.

3) PROPAGATION CHANNEL

Ranging errors are introduced by the propagation channel due to the effect of multipath, shadowing and attenuation. Certainly, multipath is the major source of ranging bias in urban environments, due to the blockage of the LoS signal. The LTE standard has typically adopted tapped-delay line (TDL) models, where a fixed power-delay profile is defined by considering time-varying channel coefficients according to a Rayleigh distribution [23]. These TDL models are called Extended Pedestrian A (EPA), Extended Vehicular A (EVA) and Extended Typical Urban (ETU), which have a delay spread of 410 ns, 2.51 μs and 5 μs with 7, 9 and 9 fixed

tap delays, respectively. The LoS probability of the EPA, EVA and ETU models is equal to $P_{\text{LoS}} = \{0.87, 0.81, 0.63\}$, respectively, by determining NLoS for those channel realisations with a first path gain (normalized by the channel gain) below -6 dB. Although advanced channels models are specified in [24], which are based on geometry-based stochastic channel models (GSCM) with non-fixed tap delays, the current standardization process still uses TDL models for the assessment of the LTE positioning capabilities. Independently of the multipath model, the macroscopic path loss and shadowing are considered within the received signal power, by computing the link budget according to general parameters defined in [24] or in [25].

4) GEOMETRY

The geometry between the BSs and the mobile device has an impact on the precision of the position calculation, known as dilution of precision (DOP). Cellular deployments are designed for optimizing the data throughput at the mobile device. This involves listening the serving BS as loud as possible while having all the neighboring BSs as silent as possible. For positioning, the requirement is completely opposite, since it is desired that the mobile device listens as many loud signals from as many neighboring BSs as possible, in order to have a good DOP. Thus, the DOP typically improves as the density of BSs increases.

D. POSITION COMPUTATION

The OTDoA position is computed by using the difference between ranging measurements from serving and neighbour BSs. The difference of pseudoranges is written as

$$\boldsymbol{\Delta\rho} = \rho_1 - \boldsymbol{\rho}, \tag{4}$$

where ρ_1 is the pseudorange between the serving BS and the mobile, and $\boldsymbol{\rho} = \left[\rho_2, \ldots, \rho_{N_{\text{BS}}}\right]^{\text{T}}$ is the vector of pseudoranges between the neighbour BSs and the mobile, being N_{BS} the number of BSs used for positioning. The classical solution of this trilateration problem is formulated as the nonlinear least squares (NLS) minimization [13], which can be solved with an iterative method, such as the Gauss-Newton (GN) algorithm [26].

One of the metrics used in this work to evaluate the positioning performance is the horizontal DOP (HDOP), which is defined for $N_{\text{BS}} \geq 3$ as

$$\text{HDOP} = \sqrt{\text{tr}\left\{\left(\mathbf{G}^{\text{T}}\mathbf{G}\right)^{-1}\right\}}, \tag{5}$$

where the geometry or Jacobian matrix of $\boldsymbol{\Delta\rho}$ is

$$\mathbf{G} = \begin{pmatrix} \frac{x-x_1}{d_1} - \frac{x-x_2}{d_2} & \frac{y-y_1}{d_1} - \frac{y-y_2}{d_2} \\ \frac{x-x_1}{d_1} - \frac{x-x_3}{d_3} & \frac{y-y_1}{d_1} - \frac{y-y_3}{d_3} \\ \vdots & \vdots \\ \frac{x-x_1}{d_1} - \frac{x-x_{N_{\text{BS}}}}{d_{N_{\text{BS}}}} & \frac{y-y_1}{d_1} - \frac{x-x_{N_{\text{BS}}}}{d_{N_{\text{BS}}}} \end{pmatrix}. \tag{6}$$

This metric helps to evaluate the precision of the position computation according to the geometry between mobile device and BSs. The previous formulation can be easily extended to the three-dimensional (3D) localization problem. However, this work focuses on the horizontal or two-dimensional (2D) problem, since the similar height of the BSs limits the ranging accuracy in the vertical axis.

Since the pseudoranges are typically biased due to the presence of multipath, the CRB of the location for biased ranging measurements has been studied in [27] and [28]. Our approach is to directly assess the OTDoA position accuracy with the root-mean-square error (RMSE) of the position error $\varepsilon_{\mathbf{x}}$, defined as

$$\text{RMSE}(\varepsilon_{\mathbf{x}}) = \sqrt{\text{E}\left[\varepsilon_{\mathbf{x}}^2\right]} = \sqrt{\text{E}\left[\|\hat{\mathbf{x}} - \mathbf{x}\|^2\right]}, \tag{7}$$

where $\varepsilon_{\mathbf{x}}$ is equal to the Euclidean distance between the mobile position $\mathbf{x}$ and the position estimation $\hat{\mathbf{x}}$. The cumulative density function (CDF) of the position error is also used to complete the positioning assessment.

III. MULTICARRIER SIGNAL AND CHANNEL MODELS

This section introduces the multicarrier signal model of the downlink, by considering a tight network synchronization and no inter-cell interference. Different joint time-delay and channel estimation models are then described.

A. MULTICARRIER SIGNAL MODEL

Given a sampling frequency F_{s}, the discrete-time multicarrier OFDM signal model is defined as

$$x_d(m) = \sqrt{\frac{2C}{N}} \sum_{n=0}^{N-1} b(n) \cdot \exp\left(j\frac{2\pi nm}{N}\right), \tag{8}$$

where C is the signal power, N is the total number of subcarriers, and $b(n)$ is the complex-valued symbol transmitted at the n-th subcarrier. The sampling period is then $T_{\text{s}} = 1/F_{\text{s}} = T/N$. After removing the CP and the carrier frequency offset, the baseband received signal is

$$y_d(m) = x_d(m) \circledast h_d(m) + n_d(m), \tag{9}$$

where $\circledast$ is the circular convolution operator, $h_d(m)$ is an unknown channel impulse response (CIR), and $n_d(m)$ is additive white Gaussian noise (AWGN). The propagation channel model is described as

$$h_d(m) = \sum_{k=0}^{L-1} h_k \cdot \text{sinc}(m - \tau_k - \tau), \tag{10}$$

where L is the number of taps of the channel, h_k is the complex gain for the k-th path, $\text{sinc}(x) = \frac{\sin(\pi \cdot x)}{\pi \cdot x}$ is the sinc function, τ_k is the tap delay relative to the first tap (i.e., $\tau_0 = 0$), and τ is the time delay introduced by the channel (i.e., the time delay of the first arriving ray).

The received signal in the frequency domain is written in matrix notation as

$$\mathbf{r} = \mathbf{B}\Gamma_\tau \mathbf{F}_L \mathbf{h} + \mathbf{w}, \tag{11}$$

where

$$\mathbf{r} = [r(-N/2+1), \ldots, r(N/2)]^T, \quad (12)$$

$$\mathbf{\Gamma} = \text{diag}\left(e^{-j\frac{2\pi}{N}(-N/2+1)\tau}, \ldots, e^{-j\frac{2\pi}{N}(N/2)\tau}\right), \quad (13)$$

$$\mathbf{B} = \sqrt{2C} \cdot \text{diag}(b(-N/2+1), \ldots, b(N/2)), \quad (14)$$

$$\mathbf{h} = [h_0, \ldots, h_{L-1}]^T, \quad (15)$$

$$\mathbf{w} = [w(-N/2+1), \ldots, w(N/2)]^T, \quad (16)$$

$\mathbf{F}_L$ is a discrete Fourier transform (DFT) matrix with $N \times L$ dimensions, defined as

$$[\mathbf{F}_L]_{n,k} = \frac{1}{\sqrt{N}} \cdot e^{-j\frac{2\pi n \tau_k}{N}}, \quad (17)$$

for $n = [-N/2+1, \ldots, N/2]$ and $k = [0, \ldots, L-1]$. The noise contribution is defined as $w(n) \sim \mathcal{CN}\left(0, \sigma_w^2\right)$ with a noise variance σ_w^2.

B. ESTIMATION MODELS

The propagation channel is assumed to be unknown, thus it has to be estimated and counteracted for accurate ranging. Since the propagation channel is modelled as in (10), the main parameters of the estimation model are the time delay τ, each tap delay τ_k, the channel coefficients $\mathbf{h}$, and the number of taps L. Several estimation models can be identified depending on the knowledge of these channel parameters, as it is introduced in [22]. The number of taps are considered a predefined parameter of the model, which can be computed with model order estimation techniques, such as the minimum description length (MDL) or Akaike methods [29].

1) $(1, L)$ MODEL

The $(1, L)$ model is formed by L periodic taps at predefined taps' delays τ_k, with the unknown parameters being τ and $\mathbf{h}$. The parameter vector to estimate is

$$\boldsymbol{\theta}_{(1,L)} = \left[\ \tau\ ,\ \text{Re}\left[\mathbf{h}^{\mathrm{T}}\right]\ ,\ \text{Im}\left[\mathbf{h}^{\mathrm{T}}\right]\ \right]^{\mathrm{T}}, \quad (18)$$

where the real and imaginary parts of the channel coefficients $\mathbf{h}$ are considered separately to obtain a real parameter vector $\boldsymbol{\theta}_{(1,L)}$. This model aims to properly characterize the channel response and to maintain a low estimation complexity, by solving a one-dimensional (1D) problem. A widely-adopted definition of the $(1, L)$ model is based on equi-spaced or periodical delay positions every sampling period T_s, i.e., $\tau_k = \{0, 1, \ldots, L-1\}$. This periodic-tap model provides a sampled version of the channel response, without the need to know the physical delays of the multipath. Still, there is a model mismatch due to the incomplete characterization of the channel response. Particularly, the close-in multipath, i.e., multipath close to the LoS signal, is not properly characterized by this $(1, L)$ periodic-tap model, which results in a degradation of the TDE performance. A simplification of this periodic-tap model is based on the use of only one estimation tap, i.e., $L = 1$ with $\tau_0 = 0$. This single-tap model results in a low computational burden, but its channel characterization is only appropriate for AWGN channel or multipath with taps' delays almost overlapped with the LoS signal.

2) (M, L) MODEL

The model mismatch of the $(1, L)$ model can be reduced by estimating a set of M taps' delays (including the time delay), where $M < L$, and by fixing the rest of taps' delays at periodic positions. Thus, the unknown parameters are the M taps' delays (also the first arriving path) and the L channel coefficients, resulting in a M-dimensional problem. As it is proposed in [22], the $(1, L)$ periodic model can be extended into the $(2, L)$ hybrid model, by defining periodic taps' delays and introducing an additional tap with unknown delay between 0 and T_s. Then, the parameter vector of the $(2, L)$ model is

$$\boldsymbol{\theta}_{(2,L)} = \left[\ \tau\ ,\ \text{Re}\left[\mathbf{h}^{\mathrm{T}}\right]\ ,\ \text{Im}\left[\mathbf{h}^{\mathrm{T}}\right]\ ,\ \tau'\ \right]^{\mathrm{T}}, \quad (19)$$

where the taps' delays are $\tau_k = \{0, \tau', 1, \cdots, L-2\}$, and τ' is the arbitrary-tap delay within a sampling period relative to the LoS signal, i.e., $0 < \tau' < 1$. This additional unknown parameter is aimed at capturing most of the close-in multipath energy. This work considers the $(2, L)$ hybrid model instead of a general (M, L) model, in order to limit the computational complexity of the TDE.

3) (L, L) MODEL

The model mismatch can be further reduced by estimating every tap delay τ_k, along the time delay τ and the channel coefficients $\mathbf{h}$. The parameter vector is

$$\boldsymbol{\theta}_{(L,L)} = \left[\ \boldsymbol{\tau}\ ,\ \text{Re}\left[\mathbf{h}^{\mathrm{T}}\right]\ ,\ \text{Im}\left[\mathbf{h}^{\mathrm{T}}\right]\right]^{\mathrm{T}}, \quad (20)$$

where $\boldsymbol{\tau} = \tau + \left[0, \tau_{c,1}, \tau_{c,2}, \ldots, \tau_{c,L-1}\right]$ is the vector of unknown taps' delays plus the time delay. Since the number of unknown parameters increases with the number of taps, the estimation problem is L-dimensional. Although the complexity of the (L, L) model increases considerably with a high number of taps, this model is estimating the actual channel response, and therefore it is of interest in order to assess the actual achievable accuracy on the TDE.

IV. CRAMÉR-RAO BOUND

The best possible accuracy of unbiased estimators can be assessed by means of the CRB for a moderate to high signal-to-noise ratio (SNR). The CRB for the joint time-delay and channel estimation is derived in this section for the channel estimation models just defined.

Given the estimation of the parameter vector $\boldsymbol{\theta} = \left[\theta_1, \theta_2, \ldots, \theta_Q\right]$, the minimum variance of any unbiased estimator $\hat{\theta}_i$ is defined by the $[i, i]$ element of the inverse of the Fisher information matrix (FIM) $\mathbf{J}(\boldsymbol{\theta})$ as

$$\text{var}\left(\hat{\theta}_i\right) \geq \text{CRB}_{i,i} = \left[\mathbf{J}^{-1}(\boldsymbol{\theta})\right]_{i,i}. \quad (21)$$

For a Gaussian problem, such as the one under analysis in (11), the $[i, j]$ element of the FIM is given by the

Bangs-Slepian formula [30],

$$[\mathbf{J}(\boldsymbol{\theta})]_{i,j} = \mathrm{tr}\left[\mathbf{C}^{-1}(\boldsymbol{\theta})\frac{\partial \mathbf{C}(\boldsymbol{\theta})}{\theta_i}\mathbf{C}^{-1}(\boldsymbol{\theta})\frac{\partial \mathbf{C}(\boldsymbol{\theta})}{\theta_j}\right] + 2\mathrm{Re}\left[\frac{\partial \boldsymbol{\mu}^{\mathrm{H}}(\boldsymbol{\theta})}{\theta_i}\mathbf{C}^{-1}(\boldsymbol{\theta})\frac{\partial \boldsymbol{\mu}(\boldsymbol{\theta})}{\theta_j}\right], \quad (22)$$

where the mean vector is $\boldsymbol{\mu}(\boldsymbol{\theta}) = \mathbf{B}\Gamma_\tau \mathbf{F}_L \mathbf{h}$, and the covariance matrix is assumed to be $\mathbf{C}(\boldsymbol{\theta}) = \mathrm{E}\left[\mathbf{w}\mathbf{w}^{\mathrm{H}}\right] = \sigma_{\mathrm{w}}^2\mathbf{I}$.

A. CRB FOR THE (1, L) MODEL

The FIM for the $(1, L)$ model is computed with the Bangs-Slepian's formula using the signal model in (11) as

$$\mathbf{J}\left(\boldsymbol{\theta}_{(1,L)}\right) = \frac{2}{\sigma_{\mathrm{w}}^2}\begin{bmatrix} J_{11} & \mathbf{J}_{21}^{\mathrm{T}} \\ \mathbf{J}_{21} & \mathbf{J}_{22}\end{bmatrix}, \quad (23)$$

where $J_{11} = \mathbf{h}^{\mathrm{H}}\mathbf{A}^{\mathrm{H}}\mathbf{D}^2\mathbf{A}\mathbf{h}$,

$$\mathbf{J}_{21} = \left[\mathrm{Im}\left[\mathbf{A}^{\mathrm{H}}\mathbf{D}\mathbf{A}\mathbf{h}\right], -\mathrm{Re}\left[\mathbf{A}^{\mathrm{H}}\mathbf{D}\mathbf{A}\mathbf{h}\right]\right]^{\mathrm{T}},$$

and

$$\mathbf{J}_{22} = \begin{bmatrix} \mathrm{Re}\left[\mathbf{A}^{\mathrm{H}}\mathbf{A}\right] & -\mathrm{Im}\left[\mathbf{A}^{\mathrm{H}}\mathbf{A}\right] \\ \mathrm{Im}\left[\mathbf{A}^{\mathrm{H}}\mathbf{A}\right] & \mathrm{Re}\left[\mathbf{A}^{\mathrm{H}}\mathbf{A}\right]\end{bmatrix},$$

being $\mathbf{A} = \mathbf{B}\mathbf{F}_L$ and $\mathbf{D} = 2\pi/N \cdot \mathrm{diag}\,(-N/2+1, \ldots, N/2)$. The CRB using the $(1, L)$ estimation model is calculated as in [31]

$$\mathbf{CRB}_{(1,L)}(\boldsymbol{\theta}_{(1,L)}) = \frac{\sigma_{\mathrm{w}}^2}{2}\begin{bmatrix} \gamma_\tau^{-1} & \mathbf{CRB}_{21}^{\mathrm{T}} \\ \mathbf{CRB}_{21} & \mathbf{CRB}_{22}\end{bmatrix}, \quad (24)$$

where $\gamma_\tau = \mathbf{h}^{\mathrm{H}}\mathbf{A}^{\mathrm{H}}\mathbf{D}\boldsymbol{\Pi}_{\mathbf{A}}^{\perp}\mathbf{D}\mathbf{A}\mathbf{h}$, being the projection matrix defined as $\boldsymbol{\Pi}_{\mathbf{A}}^{\perp} = \mathbf{I} - \mathbf{A}\left(\mathbf{A}^{\mathrm{H}}\mathbf{A}\right)^{-1}\mathbf{A}^{\mathrm{H}}$. Thus, the CRB with respect to τ is

$$\mathrm{CRB}_{(1,L)}(\tau) = \sigma_{\mathrm{w}}^2/2 \cdot \gamma_\tau^{-1}. \quad (25)$$

The resulting CRB is dependent on the channel coefficients $\mathbf{h}$, being independent of τ. The effect of the channel information on the TDE is denoted by the projection matrix $\boldsymbol{\Pi}_{\mathbf{A}}^{\perp}$. In case the channel response $\mathbf{h}$ is assumed to be known, the corresponding bound is obtained by introducing $\boldsymbol{\Pi}_{\mathbf{A}}^{\perp} = \mathbf{I}$, which results in a lower bound than $\mathrm{CRB}_{(1,L)}(\tau)$.

The expression of the CRB for the $(1, L)$ model in (25) can be applied for different predefinitions of the taps' delays, by computing the corresponding Fourier matrix as defined in (17). For instance, the $(1, 1)$ or single-tap model is a particularization of (24) for $L = 1$, i.e., $\mathbf{F}_1 = \mathbf{1}/\sqrt{N}$, which results in

$$\mathrm{CRB}_{(1,1)}(\tau) = \frac{\sigma_{\mathrm{w}}^2 \cdot N}{2 \cdot h_0^{\mathrm{H}} \cdot h_0} \cdot \left(\mathbf{b}^{\mathrm{H}}\mathbf{D}\boldsymbol{\Pi}_{\mathbf{b}}^{\perp}\mathbf{D}\mathbf{b}\right)^{-1}, \quad (26)$$

where

$$\mathbf{b} = \sqrt{2C} \cdot [b(-N/2+1), \ldots, b(N/2)]^{\mathrm{T}}, \quad (27)$$

$$\boldsymbol{\Pi}_{\mathbf{b}}^{\perp} = \mathbf{I} - \mathbf{b}\left(\mathbf{b}^{\mathrm{H}}\mathbf{b}\right)^{-1}\mathbf{b}^{\mathrm{H}}. \quad (28)$$

If the channel coefficient h_0 is considered to be known and equal to one, the CRB in (26) is equal to the general expression of the CRB for time delay in [30].

B. CRB FOR (2, L) MODEL

The parameter vector $\boldsymbol{\theta}_{(2,\mathrm{L})}$ includes one more estimate than $\boldsymbol{\theta}_{(1,L)}$, i.e., the delay τ' of a tap introduced somewhere between the first two periodic taps, in order to better represent the close-in multipath contribution. Since the Fourier matrix depends on τ', let us define

$$\mathbf{F}_{L,\tau'} = \mathbf{F}_L, \quad \text{for } \tau_k = \{0, 1, \cdots, L-2, \tau'\}. \quad (29)$$

This $(2, L)$ model is an extension of the $(1, L)$ model, thus the Fourier matrix $\mathbf{F}_L$ is substituted by $\mathbf{F}_{L,\tau'}$ in (23), and the FIM using the $(2, L)$ model results in the following partitioned matrix:

$$\mathbf{J}\left(\boldsymbol{\theta}_{(2,\mathrm{L})}\right) = \frac{2}{\sigma_{\mathrm{w}}^2}\begin{bmatrix} J_{11} & \mathbf{J}_{21}^{\mathrm{T}} & J_{31}^{\mathrm{T}} \\ \mathbf{J}_{21} & \mathbf{J}_{22} & \mathbf{J}_{23} \\ J_{31} & \mathbf{J}_{23}^{\mathrm{T}} & J_{33}\end{bmatrix} = \frac{2}{\sigma_{\mathrm{w}}^2}\left[\begin{array}{cc|c} & & J_{31}^{\mathrm{T}} \\ & \mathbf{J}\left(\boldsymbol{\theta}_{(1,\mathrm{L})}\right) & \mathbf{J}_{23} \\ \hline J_{31} & \mathbf{J}_{23}^{\mathrm{T}} & J_{33}\end{array}\right], \quad (30)$$

where

$$J_{31} = \mathrm{Re}\left[\mathbf{h}^{\mathrm{H}}\mathbf{d}\mathbf{d}^{\mathrm{T}}\mathbf{F}_{L,\tau'}^{\mathrm{H}}\mathbf{B}^{\mathrm{H}}\mathbf{D}^2\mathbf{B}\mathbf{F}_{L,\tau'}\mathbf{h}\right], \quad (31)$$

$$\mathbf{J}_{23} = \begin{bmatrix} \mathrm{Im}\left[\mathbf{F}_{L,\tau'}^{\mathrm{H}}\mathbf{B}^{\mathrm{H}}\mathbf{D}\mathbf{B}\mathbf{F}_{L,\tau'}\mathbf{d}\mathbf{d}^{\mathrm{T}}\mathbf{h}\right] \\ -\mathrm{Re}\left[\mathbf{F}_{L,\tau'}^{\mathrm{H}}\mathbf{B}^{\mathrm{H}}\mathbf{D}\mathbf{B}\mathbf{F}_{L,\tau'}\mathbf{d}\mathbf{d}^{\mathrm{T}}\mathbf{h}\right]\end{bmatrix}, \quad (32)$$

$$J_{33} = \mathbf{h}^{\mathrm{H}}\mathbf{d}\mathbf{d}^{\mathrm{T}}\mathbf{F}_{L,\tau'}^{\mathrm{H}}\mathbf{B}^{\mathrm{H}}\mathbf{D}^2\mathbf{B}\mathbf{F}_{L,\tau'}\mathbf{d}\mathbf{d}^{\mathrm{T}}\mathbf{h}, \quad (33)$$

being $\mathbf{d} = [0, \ldots, 0, 1]^{\mathrm{T}}$. The $L \times 1$ vector $\mathbf{d}$ is obtained from the derivative of the Fourier matrix $\mathbf{F}_{L,\tau'}$ with respect to τ', which is written as

$$\frac{\partial \mathbf{F}_{L,\tau'}}{\partial \tau'} = -j\mathbf{D}\mathbf{F}_{L,\tau'}\mathbf{d}\mathbf{d}^{\mathrm{T}}. \quad (34)$$

The CRB with respect to τ using the $(2, L)$ model is computed numerically as follows:

$$\mathrm{CRB}_{(2,L)}(\tau) = \left[\mathbf{J}^{-1}\left(\boldsymbol{\theta}_{(2,L)}\right)\right]_{1,1}. \quad (35)$$

C. CRB FOR (L, L) MODEL

Considering the parameter vector $\boldsymbol{\theta}_{(\mathrm{L},\mathrm{L})}$, let us define the Fourier matrix as $\mathbf{F}_{L,\boldsymbol{\tau}} = \mathbf{F}_L$ for $\tau_k = \tau_{\mathrm{c},k}$. Then, the FIM of the (L, L) model results in

$$\mathbf{J}\left(\boldsymbol{\theta}_{(L,L)}\right) = \frac{2}{\sigma_{\mathrm{w}}^2}\begin{bmatrix} \mathbf{J}_{\boldsymbol{\tau}} & \mathbf{J}_{\mathbf{h}\boldsymbol{\tau}}^{\mathrm{T}} \\ \mathbf{J}_{\mathbf{h}\boldsymbol{\tau}} & \mathbf{J}_{\mathbf{h}}\end{bmatrix}, \quad (36)$$

where

$$[\mathbf{J}_{\boldsymbol{\tau}}]_{i,j} = \mathbf{h}^{\mathrm{H}}\mathbf{d}_i\mathbf{d}_i^{\mathrm{T}}\mathbf{F}_{L,\boldsymbol{\tau}}^{\mathrm{H}}\mathbf{B}^{\mathrm{H}}\mathbf{D}^2\mathbf{B}\mathbf{F}_{L,\boldsymbol{\tau}}\mathbf{d}_j\mathbf{d}_j^{\mathrm{T}}\mathbf{h}, \quad (37)$$

$$[\mathbf{J}_{\mathbf{h}\boldsymbol{\tau}}]_i = \begin{bmatrix} \mathrm{Im}\left[\mathbf{F}_{L,\boldsymbol{\tau}}^{\mathrm{H}}\mathbf{B}^{\mathrm{H}}\mathbf{D}\mathbf{B}\mathbf{F}_{L,\tau'}\mathbf{d}_i\mathbf{d}_i^{\mathrm{T}}\mathbf{h}\right] \\ -\mathrm{Re}\left[\mathbf{F}_{L,\boldsymbol{\tau}}^{\mathrm{H}}\mathbf{B}^{\mathrm{H}}\mathbf{D}\mathbf{B}\mathbf{F}_{L,\tau'}\mathbf{d}_i\mathbf{d}_i^{\mathrm{T}}\mathbf{h}\right]\end{bmatrix}, \quad (38)$$

$$\mathbf{J}_{\mathbf{h}} = \mathbf{J}_{22}, \quad (39)$$

for $i = \{1, 2, \ldots, L\}$ and $j = \{1, 2, \ldots, L\}$, being $\mathbf{d}_i$ the i-th row of the identity matrix. As in (35), the CRB with respect to τ using the (L, L) model is computed numerically as follows:

$$\mathrm{CRB}_{(L,L)}(\tau) = \left[\mathbf{J}^{-1}\left(\boldsymbol{\theta}_{(L,L)}\right)\right]_{1,1}. \tag{40}$$

D. ECRB

Given the CRB for the channel estimation models derived in this section, the expectation of their CRB for multiple channel realizations results in the expected CRB (ECRB), which is defined as

$$\mathrm{ECRB}(\tau) = \mathrm{E}_{\mathbf{h}}\left[\mathrm{CRB}(\tau)\right]. \tag{41}$$

The computation of the ECRB can be done numerically as in this work, or it can be obtained analytically as in [32].

V. JOINT TIME-DELAY AND CHANNEL ESTIMATORS

Countermeasures against multipath are necessary in most urban environments, due to the large number of reflections and obstructions of the LoS signal. These multipath effects introduce a bias on the time-delay estimation, which significantly degrades the OTDoA positioning performance. Most of the contributions on multipath mitigation consider threshold-based or first-peak time-delay estimators, such as in [17] and [18]. These estimators are based on finding the first peak of the cross-correlation function (between received and pilot signals) above a certain threshold, which results in a low complexity. However, these data-aided schemes have a poor performance against non-resolvable multipath, such as close-in multipath, because they are only based on the correlation function. Thus, there is the need to estimate the channel, in order to counteract the effect of multipath. In this sense, joint time-delay and channel estimators can significantly improve the ranging performance, by reducing the estimation bias of the time delay. But, few contributions have addressed the joint estimation of the time-delay and channel in LTE, such as in [11] and [22].

The objective of this section is to define the general types of joint time-delay and channel estimators. Since the propagation channel is assumed to be unknown, the joint maximum likelihood (JML) approach is considered, to provide the best ranging performance in terms of minimum estimation variance. Three general types of JML estimators and one super-resolution technique are defined to counteract the effect of multipath, by using the estimation models introduced in Section III-B. These estimators use the LTE pilots dedicated for positioning, i.e., which are designed to provide an optimal channel estimation performance and high hearibility of neighbour BSs. These data-aided schemes are then able to find the time delay τ and the L channel coefficients $\mathbf{h}$ from the received signal $\mathbf{r}$ in the frequency domain, by considering L taps defined at each τ_k delay.

A. (1, L)-JML TDE

As it is derived in [22], the $(1, L)$-JML estimation of the time delay is

$$\hat{\tau} = \arg\min_{\tau}\left\{\|\mathbf{P}^{\perp}_{\mathbf{A},\tau}\mathbf{r}\|^2\right\}, \tag{42}$$

where $\mathbf{P}^{\perp}_{\mathbf{A},\tau} = \mathbf{I} - \mathbf{A}_\tau\left(\mathbf{A}_\tau^H\mathbf{A}_\tau\right)^{-1}\mathbf{A}_\tau^H$ is the orthogonal projection matrix onto the subspace orthogonal to that spanned by the columns of $\mathbf{A}_\tau$, which is $\mathbf{A}_\tau = \mathbf{B}\Gamma_\tau\mathbf{F}_L$. This work focuses on the periodic-tap estimation model, i.e., $\tau_k = \{0, 1, \ldots, L-1\}$, in order to capture most of the multipath energy with L estimation taps. The number of taps is assumed to be estimated in a previous stage. Considering $L = 1$, the $(1, 1)$-JML estimator results in finding the maximum peak of the cross-correlation function. If there is a fine synchronization and the estimation range is appropriately bounded, this $(1, 1)$-JML estimator can be approximated by threshold-based or first-peak estimators [17], [18].

B. (2, L)-JML TDE

The $(2, L)$-JML estimator is an extension of the $(1, L)$-JML estimator that is aimed at counteracting close-in multipath. Let us consider the hybrid-tap estimation model introduced in [22] with $\tau_k = \left\{0, \tau', 1, \cdots, L-2\right\}$ for $0 < \tau' < 1$. The $(2, L)$-JML TDE is then defined as

$$\begin{bmatrix}\hat{\tau}\\ \hat{\tau}'\end{bmatrix} = \arg\min_{\tau,\tau'}\left\{\|\mathbf{P}^{\perp}_{\mathbf{A},\tau,\tau'}\mathbf{r}\|^2\right\}, \quad \text{s.t. } 0 < \tau' < 1, \tag{43}$$

where $\mathbf{P}^{\perp}_{\mathbf{A},\tau,\tau'} = \mathbf{I} - \mathbf{A}_{\tau,\tau'}\left(\mathbf{A}^H_{\tau,\tau'}\mathbf{A}_{\tau,\tau'}\right)^{-1}\mathbf{A}^H_{\tau,\tau'}$, and $\mathbf{A}_{\tau,\tau'} = \mathbf{B}\Gamma_\tau\mathbf{F}_{L,\tau'}$. This estimator is designed to provide a better characterization of close-in multipath than the $(1, L)$-JML estimator, at the expense of a slightly higher computational burden.

C. (L, L)-JML TDE

The derivation of the (L, L)-JML estimator is also extended from the $(1, L)$-JML estimator, resulting in an optimization problem of order L. The (L, L)-JML TDE is then defined as

$$\hat{\boldsymbol{\tau}} = \arg\min_{\boldsymbol{\tau}}\left\{\|\mathbf{P}^{\perp}_{\mathbf{A},\boldsymbol{\tau}}\mathbf{r}\|^2\right\}, \tag{44}$$

where $\mathbf{P}^{\perp}_{\mathbf{A},\boldsymbol{\tau}} = \mathbf{I} - \mathbf{A}_{\boldsymbol{\tau}}\left(\mathbf{A}^H_{\boldsymbol{\tau}}\mathbf{A}_{\boldsymbol{\tau}}\right)^{-1}\mathbf{A}^H_{\boldsymbol{\tau}}$, and $\mathbf{A}_{\boldsymbol{\tau}} = \mathbf{B}\Gamma_\tau\mathbf{F}_{L,\boldsymbol{\tau}}$. As a result, the (L, L)-JML estimator is expected to have a very high computational burden as L increases.

D. (L, L)-ESPRIT TDE

Super-resolution techniques have a lower complexity than the ML approach, thus they are typically considered to solve the (L, L) estimation problem. As in [11], the estimation of signal parameters via rotational invariance techniques (ESPRIT) algorithm is used to estimate the time delay with the (L, L) model. This method is based on staggered subspaces or snapshots of the channel estimates, i.e., $\hat{H}(n) = b^*(n) \cdot r(n)$,

which are used to form the so-called data matrix [33]. In [11], the data matrix is defined as

$$\mathbf{X} = [\boldsymbol{x}_0, \cdots, \boldsymbol{x}_{P-1}]^{\mathrm{T}}, \tag{45}$$

$$\boldsymbol{x}_p = \left[\hat{H}_{\mathrm{PRS}}(p), \cdots, \hat{H}_{\mathrm{PRS}}(p+M-1)\right]^{\mathrm{T}}, \tag{46}$$

where $\mathbf{X}$ is a $P \times M$ matrix with $P = 2 \cdot N_{\mathrm{RB}} - M$, $\hat{H}_{\mathrm{PRS}}(p) = \hat{H}(n)$ for $p = \{0, \cdots, P-1\}$ and $n \in \mathcal{N}_{\mathrm{PRS}}$, being $\mathcal{N}_{\mathrm{PRS}}$ the subset of PRS subcarrier indexes, and $L \leq M < N_{\mathrm{RB}}$. A high value of M reduces the impact of noise, due to an increased number of averaged samples, but it degrades the estimation resolution of the taps' delays [20]. As it is described in [33], the total least squares (TLS) is based on the singular value decomposition (SVD) of the data matrix, which is written as $\mathbf{X} = \mathbf{U}\boldsymbol{\Sigma}\mathbf{V}^{\mathrm{H}}$. First, the subspace $\mathbf{V}$ is partitioned as

$$\mathbf{V}_{\mathrm{s}} = \mathbf{V} \cdot [\mathbf{I}_{L\times L}\ \mathbf{0}_{L\times M-L}]^{\mathrm{T}}, \tag{47}$$

$$\mathbf{V}_{\mathrm{s},1} = [\mathbf{I}_{M-1\times M-1}\ \mathbf{0}_{M-1\times 1}] \cdot \mathbf{V}_{\mathrm{s}}, \tag{48}$$

$$\mathbf{V}_{\mathrm{s},2} = [\mathbf{0}_{M-1\times 1}\ \mathbf{I}_{M-1\times M-1}] \cdot \mathbf{V}_{\mathrm{s}}. \tag{49}$$

Then, these two subspaces $\mathbf{V}_{\mathrm{s},1}$ and $\mathbf{V}_{\mathrm{s},2}$ are staggered, and a SVD is performed as $\left[\mathbf{V}_{\mathrm{s},1}\ \mathbf{V}_{\mathrm{s},2}\right] = \tilde{\mathbf{U}}\tilde{\boldsymbol{\Sigma}}\tilde{\mathbf{V}}^{\mathrm{H}}$, where $\tilde{\mathbf{V}}$ is partitioned in $L \times L$ quadrants, i.e.,

$$\tilde{\mathbf{V}} = \begin{bmatrix} \tilde{\mathbf{V}}_{11} & \tilde{\mathbf{V}}_{12} \\ \tilde{\mathbf{V}}_{21} & \tilde{\mathbf{V}}_{22} \end{bmatrix}. \tag{50}$$

Given the TLS solution $\boldsymbol{\Psi} = -\tilde{\mathbf{V}}_{12}\tilde{\mathbf{V}}_{22}^{-1}$, the time delay and taps' delays are finally computed as

$$\hat{\boldsymbol{\tau}} = \frac{N_{\mathrm{RS}}}{12\pi} \cdot \arg\{\boldsymbol{\psi}\}, \tag{51}$$

where $\boldsymbol{\psi} = [\psi_0, \cdots, \psi_{L-1}]$ are the L eigenvalues of $\boldsymbol{\Psi}$.

Notice that (45) does not consider the empty DC subcarrier of the LTE downlink transmission and the PRS allocation. This results in an estimation bias due to the additional subcarrier that separates the two center PRS pilots. As it is verified through simulations, this bias is practically negligible as the signal bandwidth increases. Thus, (45) is a valid approximation for the application of the ESPRIT algorithm in realistic LTE conditions.

VI. SIMULATION RESULTS

This section assesses the ranging performance of joint time-delay and channel estimators in representative multipath environments. These estimators are the (1, 1)-JML, $(1, L)$-JML, $(2, L)$-JML, and (L, L)-ESPRIT. The evaluation considers the signal bandwidth, multipath delay spread, C/N_0 and the number of estimated taps, in order to provide insights on the use of the most adequate time-delay estimator for a certain multipath scenario.

The TDE is performed with only one OFDM symbol, assuming a coherent multipath channel over this period. Since one OFDM symbol is the minimum integration time, the results provide a worst-case performance assessment. The TDE measurements are assumed to be obtained by a positioning receiver, which is expected to track the received signal. Thus, a fine synchronization is considered, resulting in frequency offsets almost negligible and a TDE range within one sampling period, i.e., $\tau \in [-1/2, 1/2]$ in T_{s} units. In these conditions, the ranging performance of widely-adopted threshold-based estimators is practically equivalent to the performance of the (1, 1)-JML estimator. In the case of the (L, L)-ESPRIT algorithm, $M = N_{\mathrm{RB}} - 1$ is considered to average the maximum number of samples, and to reduce the noise contribution.

A. ATTAINABILITY OF THE CRB

The CRB expressions derived in Section IV are first assessed by considering a multipath channel with periodic taps. This helps to evaluate the attainability of the CRB by using the different estimation models. The multipath channel is then defined as

$$h_d(m) = \frac{1}{\|\mathbf{h}\|} \sum_{k=0}^{L-1} h_k \cdot \mathrm{sinc}(m - \Delta\tau \cdot k - \tau), \tag{52}$$

where $\Delta\tau$ is the tap-delay separation, $h_k = e^{-\frac{k}{L}}$ and $\mathbf{h} = [h_0, \cdots, h_{L-1}]^{\mathrm{T}}$. The tap-delay separation is a parameter defined to assess the effect of the multipath overlapping. The channel coefficients $\mathbf{h}$ are defined by fixed exponential decaying values, in order to force a multipath realisation with LoS conditions, since the CRB expressions do not consider any NLoS bias.

Let us consider $C/N_0 = 90$ dB-Hz and an LTE system bandwidth of 10 MHz (i.e., $N_{\mathrm{RB}} = 50$), which results in SNR $= C/N_0 - 10\log_{10}(B_{\mathrm{RS}}) = 20.49$ dB. This is a typical SNR level for a macro-cell deployment. Under these assumptions, the square root of each CRB is computed as a function of the tap-delay separation for $L = \{1, 4, 16\}$ in Figure 1. For $\Delta\tau < 1$, there is a high CRB because there is a high overlapping between multipath components and the problem becomes ill-conditioned. For $\Delta\tau > 1$, the multipath overlapping is only due to the side lobes of the sinc function in (52). Thus, the overlapping effect is mainly significant for $0 < \Delta\tau < 2$. In addition, the CRB increases with the number of taps L and the number of estimated taps' delays, as a consequence of the larger number of unknowns to be determined. For this reason, the highest CRB is obtained for the (L, L) estimation model. But, the degradation of the CRB is not linear with the number of taps' delays to be estimated. For instance, the square root of the CRB for (1,4), (2,4) and (4,4) models at $\Delta\tau = 1$ is approximately 0.4, 0.5 and 2.4 meters, respectively.

Let us now focus on the case of $L = 4$ and $\Delta\tau = 1$. The CRB is evaluated for $50 < C/N_0 < 120$ dB-Hz and the three estimation models. This range of C/N_0 values is consistent with realistic levels of an LTE deployment, as it is confirmed by the experimental results in Section VII-A. The RMSE of the (1, 1)-JML, $(1, L)$-JML, $(2, L)$-JML, (L, L)-JML and (L, L)-ESPRIT estimators is then computed with 1000 Monte-carlo simulations. As it is shown in Figure 1b, the JML estimators for $L > 1$ attain their

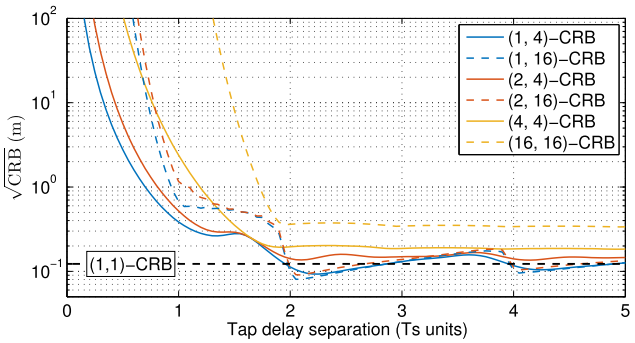

(a)

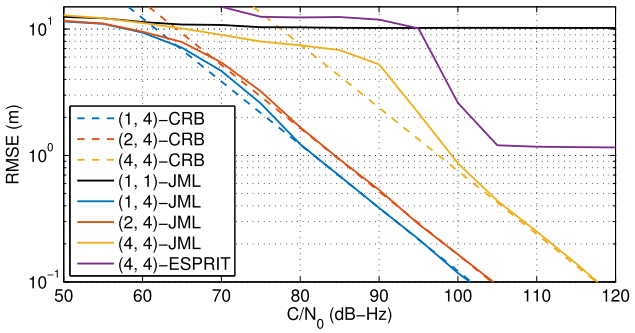

(b)

FIGURE 1. Ranging performance for each estimation model and a 10-MHz LTE system bandwidth, by considering a multipath channel with equi-spaced taps' delays and exponential-decaying coefficients. (a) CRB for $L = \{1, 4, 16\}$ and $C/N_0 = 90$ dB-Hz. (b) CRB and RMSE for $L = 4$ and $\Delta\tau = 1$.

corresponding CRB for the moderate- and high-C/N_0 region, and their RMSE depart from the CRB at different C/N_0 depending on the estimation model. The (1, 1)-JML estimator has the worst performance, due to its very limited counteraction of multipath. The best performance is achieved by the $(1, L)$-JML estimator. This confirms that the $(1, L)$ model is the best solution, if multipath can be properly characterized by periodic taps' delays. Since the (L, L)-ESPRIT estimator is biased, it departs from the (L, L)-CRB. But, the bias of the ESPRIT algorithm is significantly low, and it is more computational efficient than the (L, L)-JML estimator. Thus, the (L, L) model is only evaluated with the ESPRIT algorithm.

Further simulations have also validated the attainability of the JML estimators to the ECRB for 1000 multipath realisations, but these results are not shown here due to space limitations. This attainability is fulfilled for moderate to high C/N_0 if there is no mismatch between the estimation model and the propagation channel model, otherwise the model mismatch causes a degradation on the estimation performance.

B. ACHIEVABLE RANGING ACCURACY

The multipath model defined in (52) by periodic taps has helped to assess the effect of the multipath overlapping, the model mismatch and the number of estimated taps.

TABLE 2. Number of taps L optimized for standard EPA and ETU channel models at $C/N_0 = 90$ dB-Hz.

Signal BW (MHz)	(1, L)-JML		(2, L)-JML		(L, L)-ESPRIT	
	EPA	ETU	EPA	ETU	EPA	ETU
1.02	2	6	2	7	1	2
2.64	2	7	3	8	1	5
4.44	2	8	3	9	2	6
8.94	2	4	2	5	2	7
13.44	3	4	4	22	3	7
17.94	4	10	5	11	3	8

The achievable ranging accuracy of the estimators is now studied with standard TDL channel models for an LTE system bandwidth from 1.4 to 20 MHz and moderate C/N_0 equal to 90 dB-Hz. These TDL models characterize representative urban channels for a macro-cell deployment. The EPA and ETU models, defined in [23], are considered because their simplicity helps to ease the reproducibility of the results, and they are widely adopted in the LTE standardization. In addition, the use of EPA and ETU models allows a performance assessment of the estimators with low and high delay spread of the multipath channel, respectively.

The right selection of L helps in properly capturing the feature characteristics of the multipath impulse response to be estimated. The estimation model should then consider the range of delays where the multipath energy is concentrated. If there is no knowledge of the delay spread, L can be selected assuming a worst-case scenario as $L = \lceil T_{\mathrm{CP}} \cdot N_{\mathrm{RS}}/T_{\mathrm{s}} \rceil$, using the normal CP length of $T_{\mathrm{CP}} = 4.7\mu$s indicated in the LTE standard. The disadvantage of periodic-tap models is that some of these fixed taps may barely capture any multipath contribution. This might be caused by the sparse distribution of the actual taps to be estimated, or to situations where the delay spread is much shorter than the one expected. This limitation can be circumvented by using an (L, L) model instead, where L taps positions are estimated to better match the actual channel. Our design criteria for L is to use the smallest number of taps, in order to capture most of the channel energy.

Let us consider $C/N_0 = 90$ dB-Hz as a realistic value for an outdoor macro-cell scenario, as it is experimentally obtained in Section VII-A. The minimum L to achieve the minimum ranging error is computed through Monte-carlo simulations, and summarized in Table 2 for the LTE signal bandwidths. The low delay spread of the EPA model results in a lower L with respect to the high delay spread of the ETU model. As the signal bandwidth increases, there are more resolvable multipath components, and L increases as well to capture the multipath contribution. The RMSE of the estimators is shown in Figure 2. The best ranging performance is obtained with the $(1, L)$-JML and $(2, L)$-JML algorithms in most of the cases, because they are more robust against noise with respect to the (L, L)-ESPRIT, and more accurate than the (1, 1)-JML or threshold-based estimators. The results show that a reduced L is effective to counteract the high

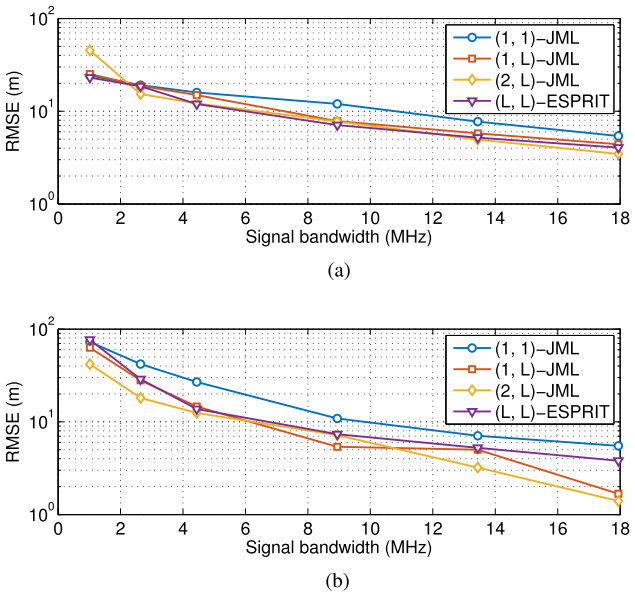

FIGURE 2. RMSE of the different ranging estimators for every LTE signal bandwidth at $C/N_0 = 90$ dB-Hz, computed with 1000 Monte-carlo simulations. (a) EPA channel model. (b) ETU channel model.

TABLE 3. 50%-CDF of ranging errors at $C/N_0 = 90$ dB-Hz.

BW (MHz)	50%-CDF of ranging error (m) for EPA channel			
	(1, 1)-JML	(1, L)-JML	(2, L)-JML	(L, L)-ESPRIT
1.02	13.37	**12.76**	21.96	13.55
2.64	14.56	14.57	**11.10**	14.43
4.44	14.39	11.86	12.59	**11.25**
8.94	11.46	8.56	8.29	**6.95**
13.44	7.89	4.13	4.14	**3.97**
17.94	6.08	3.12	**3.01**	4.07
BW (MHz)	**50%-CDF of ranging error (m) for ETU channel**			
	(1, 1)-JML	(1, L)-JML	(2, L)-JML	(L, L)-ESPRIT
1.02	62.51	54.76	**32.92**	61.82
2.64	43.48	24.18	**14.96**	24.60
4.44	31.25	13.45	13.76	**11.79**
8.94	11.01	**5.72**	12.27	7.33
13.44	6.35	5.73	**4.58**	5.21
17.94	5.59	6.10	6.75	**3.80**

overlapping multipath, such as with the EPA model, while an increased L can be used with more resolvable multipath, such as with the sparse ETU model. In order to further highlight the performance improvement due to multipath counteraction, the CDF of the ranging error is computed, and the 50% and 95% values are summarized in Table 3 and 4, respectively, where the values in bold correspond to the minimum ranging error for each bandwidth. The 50%-CDF metric especially shows the importance of using joint time-delay and channel estimation to achieve a ranging accuracy around two times better than with conventional estimators, in most of the cases of Table 3. In contrast, these multipath mitigation techniques provide almost no improvement against NLoS bias, as it is shown with the 95%-CDF metric in Table 4. According to the results obtained, an LTE system with a 10-MHz bandwidth

TABLE 4. 95%-CDF of ranging errors at $C/N_0 = 90$ dB-Hz.

BW (MHz)	95%-CDF of ranging error (m) for EPA channel			
	(1, 1)-JML	(1, L)-JML	(2, L)-JML	(L, L)-ESPRIT
1.02	**140.03**	140.80	143.23	141.08
2.64	52.38	53.78	54.92	**51.24**
4.44	32.72	**31.25**	32.38	32.71
8.94	>16.77	**15.38**	>16.77	>16.77
13.44	>11.15	**10.34**	10.68	>11.15
17.94	>8.36	**7.69**	8.06	>8.36
BW (MHz)	**95%-CDF of ranging error (m) for ETU channel**			
	(1, 1)-JML	(1, L)-JML	(2, L)-JML	(L, L)-ESPRIT
1.02	>146.96	**132.26**	139.52	>146.96
2.64	>56.78	51.83	**46.18**	>56.78
4.44	>33.76	**31.99**	32.41	>33.76
8.94	>16.77	**16.06**	>16.77	>16.77
13.44	>11.15	**10.78**	10.89	>11.15
17.94	>8.36	>8.36	>8.36	>8.36

provides a ranging accuracy on the order of 10 meters. This applies to the case when standard EPA and ETU multipath channel models are considered, and optimal joint time-delay and channel estimation techniques are applied at the user terminal.

The LTE position accuracy is expected to improve in indoor femtocell scenarios or vehicle-to-infrastructure (V2I) highway scenarios, due to a multipath channel with lower delay spread and higher SNR level than the outdoor urban macro-cell scenario. In addition, the ESPRIT algorithm is expected to improve its positioning performance as the effect of the multipath overlapping decreases, such as the large bandwidths expected in 5G networks. A good trade-off is achieved by the $(1, L)$-JML estimator for limited bandwidths, e.g. at sub-6 GHz bands, when L is set to characterize most of the multipath contribution.

VII. LABORATORY EXPERIMENTS

The objective of this section is to discuss the positioning robustness in LTE, by considering the minimum number of resources available. That is, OTDoA measurements from three BSs (i.e., $N_{\text{BS}} = 3$) using only one OFDM symbol. In addition, tight network synchronization and negligible inter-cell interference are assumed, in order to obtain a lower bound of the achievable performance in practice. For this purpose, an experimental testbed is implemented for an LTE system bandwidth of 1.4 and 10 MHz. A controlled scenario is emulated for static mobile positions in a typical macro-cell deployment, and the time and frequency synchronization errors of the testbed are removed with a calibration signal. Thus, the assessment is based on the impact of multipath and geometry between BSs. The $(1, L)$-JML and $(2, L)$-JML estimators are used with the corresponding L values of Table 2. Given the expected C/N_0 values and the low signal bandwidths, the (L, L)-ESPRIT algorithm is not considered due to its worse RMSE with respect to the other estimators, and the $(1, 1)$-JML estimator is used to represent widely-adopted threshold-based estimators.

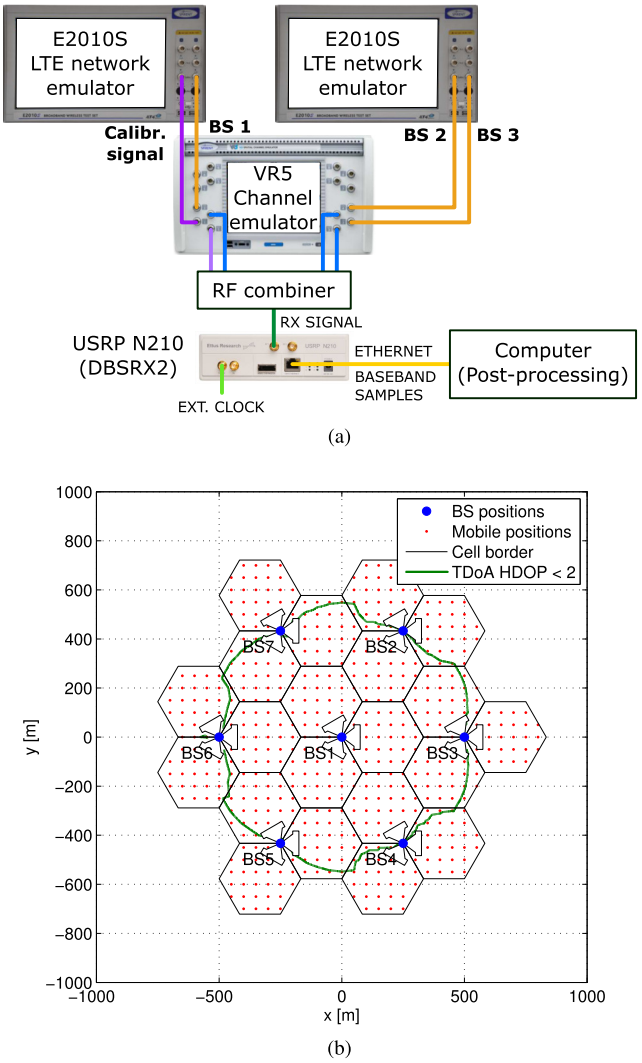

FIGURE 3. Experimental testbed at the European Navigation Laboratory (ENL) of the European Space Agency in ESTEC (The Netherlands), in order to emulate an LTE network deployment with 7 BSs and ISD of 500 meters. (a) Laboratory testbed. (b) LTE network deployment.

A. LABORATORY TESTBED

The experiments are conducted at the European Navigation Laboratory (ENL) of the European Space Agency in ESTEC (The Netherlands). The laboratory testbed is based on the emulation of an outdoor macro-cell network and the estimation of the mobile device with a software receiver. A diagram of this testbed is shown in Figure 3a. The experimental scenario is based on the typical hexagonal cellular deployment with inter-site distance (ISD) equal to 500 meters. The resulting cell layout is shown in Figure 3b, where the region with a HDOP below 2 is also depicted. An LTE network simulator is first used to compute the propagation losses between each mobile position and BS, with the standard model in [25] for a carrier frequency of 816 MHz. The three most powerful BSs at each mobile position are only considered for emulation.

Two Spirent E2010S LTE network emulators are configured to transmit downlink signals from four BSs with a system bandwidth of 1.4 or 10 MHz. One of the BSs is used for calibration purposes, being its signal only affected by AWGN. The Spirent VR5 HD spatial channel emulator applies the pre-computed propagation losses and the ETU channel model to the three other BSs. The combined output signals are then down-converted and sampled to baseband by the USRP N210 with DBSRX2 daughterboard, which is connected to a stable reference clock. Our MATLAB-based LTE software receiver [34] post-processes the baseband signal, which is re-sampled from 10 and 25 Msps to 1.92 and 15.36 Msps for the 1.4- and 10-MHz system bandwidth, respectively. Similarly to [16], the CRS of the calibration BS is used to acquire and track the receiver clock offset. Therefore, the ranging errors are only affected by multipath and noise, and they can be directly computed from the ranging estimates. This TDE is performed with the $(1, 1)$-JML, $(1, L)$-JML and $(2, L)$-JML estimators within a range of one sampling period, i.e., $\hat{\tau} \in [-1/2, 1/2]$ in T_s units. Since the true time delay τ is precisely tracked with the calibration signal, the ToA measured distance or observed pseudorange of the i-th BS is then computed as $\rho_i = d_i + c \cdot \hat{\tau}_i$, where $\hat{\tau}_i$ is the TDE from the CRS symbol of the i-th BS. The OTDoA measurements are finally obtained as in (4), and each mobile position is calculated with 10 iterations of the GN algorithm described in [26]. The initial position estimate used for this iterative algorithm is at the barycentre of the three most powerful BSs.

According to the grid of points depicted in Figure 3b, there are 599 different static mobile positions, where each position is emulated during 20 radio frames. For each radio frame, there is an SNR estimation obtained with the non-data-aided technique in [35]. The probability density function (PDF) of the resulting C/N_0 estimation is shown in Figure 6. The serving BS is more powerful than the neighbour BSs by around 10 and 15 dB, respectively. The C/N_0 levels are above 60 dB-Hz, and the corresponding serving BS level is typically between 80 and 90 dB-Hz, being its average C/N_0 closer to the latter value. The differences on the C/N_0 estimates between both system bandwidths are mainly due to the calibration of the USRP gain. These C/N_0 estimates are then used to calibrate the pre-computed propagation losses, which do not consider the receiver losses.

B. RANGING PERFORMANCE

The ranging performance of the estimators is assessed with measurements from the laboratory experiment and benchmarked with the results obtained by simulation in Section VI-B. In the experimental case, the ranging measurements are sorted according to the expected C/N_0 of the emulated scenario. The RMSE of the TDE is then computed as function of the C/N_0 with a resolution of 5 dB-Hz. In the simulated case, the RMSE is calculated with 1000 Monte-carlo realisations for each C/N_0 value. The results for a 1.4- and 10-MHz system bandwidth (i.e., 6 and 50 RBs, respectively) are shown in Figure 5. The experimental results are in line with the simulations of Section VI-B,

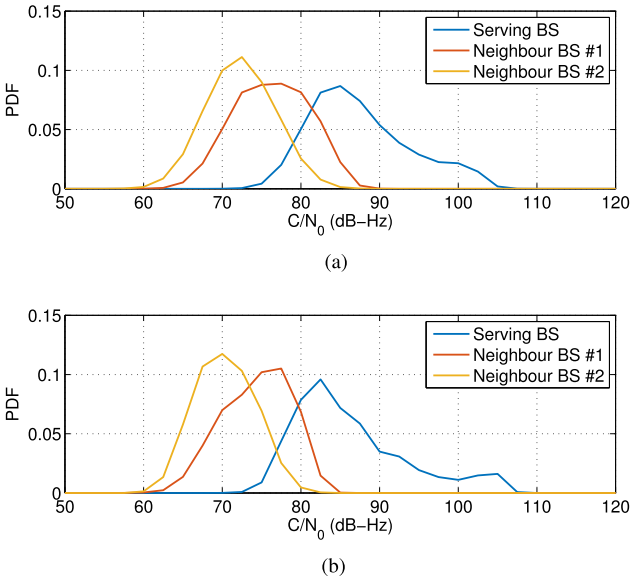

FIGURE 4. PDF of the C/N_0 estimates obtained with the captured laboratory signals over ETU multipath channel. (a) 1.4-MHz system bandwidth with 6 RBs of PRS. (b) 10-MHz system bandwidth with 50 RBs of PRS.

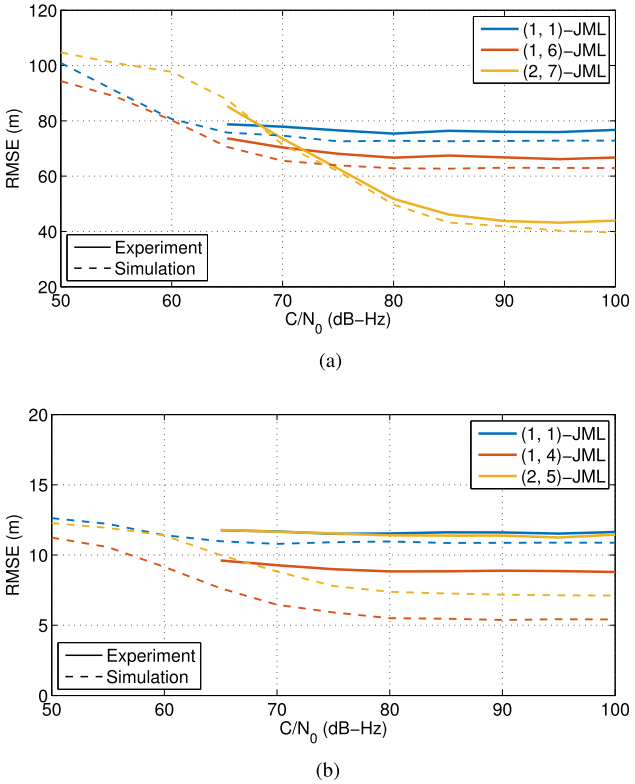

FIGURE 5. Experimental and simulated RMSE of time-delay estimators over ETU multipath channel. (a) 1.4-MHz system bandwidth with 6 RBs of PRS. (b) 10-MHz system bandwidth with 50 RBs of PRS.

because the $(2, L)$-JML and $(1, L)$-JML estimators obtain the best ranging performance for 6 and 50 RBs, respectively. According to these results, the achievable ranging accuracy

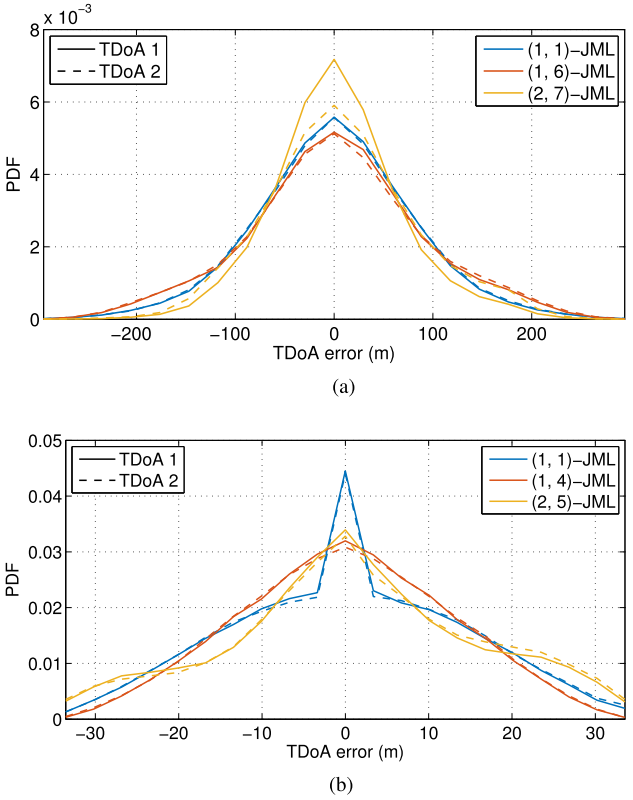

FIGURE 6. PDF of the TDoA error obtained with the laboratory experiment over ETU multipath channel. (a) 1.4-MHz system bandwidth with 6 RBs of PRS. (b) 10-MHz system bandwidth with 50 RBs of PRS.

is close to 40 meters for $N_{\mathrm{RB}} = 6$ RBs, and slightly below 10 meters for $N_{\mathrm{RB}} = 50$ RBs. Still, there is a bias on the achievable accuracy between experiment and simulation. For instance, considering $C/N_0 = 90$ dB-Hz, this difference is between 1 and 4 meters for the JML estimators in both bandwidth configurations. This bias is mainly due to the ideal filter response assumed in the simulations, which is considered to be rectangular. As it is shown in [34], the non-rectangular filter response of the USRP affects the achievable ranging accuracy of the estimators.

The TDoA error is now assessed for the two pairs of TDE experimental measurements. The PDF of the TDoA errors is shown in Figure 6, where a Gaussian-like distribution is observed, as it could be expected from [14] and [15], except for the (2, 5)-JML estimator in the 50-RBs case. The (2, 7)-JML estimator for 6 RBs and (1, 4)-JML estimator for 50 RBs obtain a higher density of errors around zero than the other estimators, resulting in a better ranging accuracy. But, in contrast to the RMSE of the TDE, the (1, 1)-JML estimator is the second best estimator in terms of TDoA error. This is due to the fact that common outliers present in individual measurements tend to cancel out when computing differential measurements. This effect is more noticeable for 50 RBs due to the dense multipath contribution at the estimation boundary, as it can be seen in Figure 6b. Thus, these bounded outlier estimations result in erroneous TDoA measurements.

TABLE 5. Experimental positioning results with 3 BSs for mobile locations with HDOP ≤ 2.

System BW (MHz)	JML est.	Prob. avail. (%)	RMSE (m)	CDF (m)		
				50%	67%	95%
1.4	$(1,1)$	74.2	64.4	66.3	104.5	>147
	$(1,L)$	83.7	72.4	68.7	96.5	>147
	$(2,L)$	84.7	62.6	56.1	79.7	>147
10	$(1,1)$	31.0	9.8	>16.8	>16.8	>16.8
	$(1,L)$	73.3	9.8	11.1	14.8	>16.8
	$(2,L)$	44.4	10.0	>16.8	>16.8	>16.8

TABLE 6. Experimental positioning results with 3 BSs for mobile locations with HDOP > 2.

System BW (MHz)	JML est.	Prob. avail. (%)	RMSE (m)	CDF (m)		
				50%	67%	95%
1.4	$(1,1)$	33.0	88.1	>147	>147	>147
	$(1,L)$	34.0	91.3	>147	>147	>147
	$(2,L)$	38.2	88.3	>147	>147	>147
10	$(1,1)$	6.8	10.9	>16.8	>16.8	>16.8
	$(1,L)$	16.4	10.9	>16.8	>16.8	>16.8
	$(2,L)$	10.0	10.7	>16.8	>16.8	>16.8

In this sense, this work does not use the outlier TDE measurements for computing the mobile position, and the position estimation is left as not available for those situations.

C. POSITIONING PERFORMANCE

The LTE positioning capabilities are evaluated with the experimental ranging measurements of the $(1,1)$-JML, $(1,L)$-JML and $(2,L)$-JML estimators. The OTDoA ranging measurements from 3 BSs are used with 10 iterations of the GN algorithm to compute the position. Since the position accuracy strongly depends on the geometry between the used BSs and the mobile device, a region of good geometry is depicted in Figure 3b. This region is defined by a HDOP $\leq$ 2, thus a mobile position with HDOP $>$ 2 is here considered to have a deficient geometry. Then, the positioning performance is assessed depending on the HDOP at each mobile position. As it is discussed in the previous section, the outlier TDE measurements may result in an erroneous position estimation, and they corrupt the assessment of the positioning performance. Thus, the position estimation is left as unavailable if there is an outlier estimation. Then, the probability of position availability is here defined as $P\left(\varepsilon_{\mathbf{x}} < c \cdot T_s/2, |\hat{\tau}_k| \leq 0.49 \mid k\right)$, i.e., the position solution is available if the position error has converged below half sampling period (i.e., below 147 and 16.8 meters for 6 and 50 RBs, respectively), and there is no outlier TDE. Then, the RMSE is computed considering these available position solutions. In addition, the CDF of the position error is calculated over the interval between 0 and half sampling period, i.e., $P\left(0 < \varepsilon_{\mathbf{x}} < c \cdot T_s/2\right)$. These positioning metrics are shown for good geometry regions (HDOP $\leq$ 2) in Table 5 and deficient geometry regions (HDOP $>$ 2) in Table 6. The CDF of the position errors can be seen for the different cases in Figure 7. For a small bandwidth and bad geometry, there is no advantage to use more elaborated estimators than $(1,1)$-JML or threshold-based estimators, due to the coarse achievable position accuracy. If there is a good geometry, but small bandwidth, the $(2,L)$-JML estimator helps to achieve a position accuracy around 80 meters on the 67% of the time, due to its counteraction of close-in multipath. The advantage of using advanced estimators is even more notorious for large bandwidths, due to the reduced effect of the multipath overlapping. Thus, the $(1,L)$-JML estimator is able to

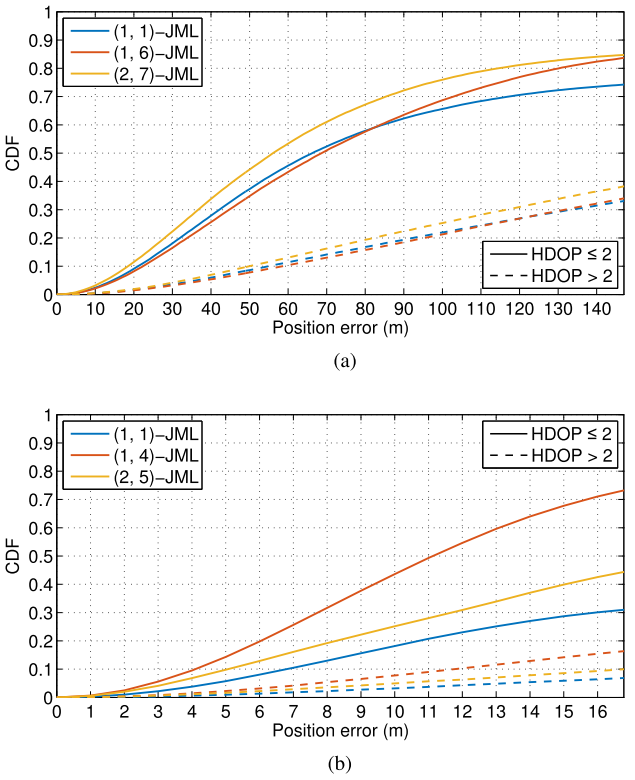

FIGURE 7. Position error with experimental OTDoA ranging measurements from 3 BSs for the mobile locations with HDOP ≤ 2 and HDOP > 2. (a) 6 RBs. (b) 50 RBs.

achieve the best positioning performance. As it is shown in Table 5 for a 10-MHz system bandwidth, the position accuracy (i.e., RMSE) of the $(1,4)$-JML estimator is around 10 meters for the 73% of the position fixes, as compared to just 31% of the occasions for the simple $(1,1)$-JML estimator.

These experimental results show the position robustness of each ranging estimator, when assuming a minimum number of resources, i.e., 3 BSs and TDE with one OFDM symbol. In addition, the results are in line with the theoretical and simulation results obtained in Section VI. The adequate channel characterization is essential to reduce the number of outlier TDE measurements, in order to obtain an accurate position solution. In this sense, the $(1,L)$-JML estimators achieve a good robustness for each system bandwidth, with a probability of position availability between 70% and 80%

with good HDOP. Thus, the $(1, L)$-model can be used to design a robust ranging estimator able to target a position accuracy within half sampling period for a limited system bandwidth, by assuming minimum positioning resources.

VIII. CONCLUSIONS

This paper has analysed the achievable ranging capabilities of different time-delay estimators able to counteract multipath, and their application to Long Term Evolution (LTE) mobile localization. Since future fifth generation (5G) cellular networks are expected to adopt similar features of the LTE physical layer, such as the multicarrier signal, this assessment is considered a testbench for the design of cellular-based localization applications with limited bandwidth at sub-6 GHz bands, by using minimal positioning resources. The multipath counteraction is based on the joint time-delay and channel estimation, and their achievable ranging performance is assessed by deriving the corresponding Cramér-Rao Bound (CRB). The theoretical and simulation results show that periodic-tap joint maximum likehood (JML) approaches achieve a better ranging performance than threshold-based and super-resolution techniques. Then, laboratory results are provided to assess the practical performance of JML estimators with a time-difference of arrival (TDoA) positioning method, for an LTE system bandwidth of 1.4 and 10 MHz. The experimental results show that the most robust JML estimator is also based on a periodic channel estimation model, given pre-computed number of estimation taps. The horizontal position accuracy obtained by this estimator is around 10 meters for the 73% of the position fixes, with a 10-MHz system bandwidth and good position geometry. This confirms the feasibility to achieve a position accuracy within half sampling period, given the appropriate design of the number of periodic estimation taps with a JML approach. Future work is aimed at studying the exploitation of antenna arrays for precise and reliable cellular localization.

ACKNOWLEDGMENT

The content of the present article reflects solely the authors' view and by no means represents the official European Space Agency (ESA) view.

REFERENCES

[1] J. A. del Peral-Rosado, R. Raulefs, J. A. López-Salcedo, and G. Seco-Granados, "Survey of cellular mobile radio localization methods: From 1G to 5G," *IEEE Commun. Surveys Tuts.*, vol. 20, no. 2, p. 25, 2nd Quart., 2018.

[2] "Fourth report and order on wireless E911 location accuracy requirements," Fed. Commun. Commiss., Washington, DC, USA, Tech. Rep. FCC-15-9, Jan. 2015.

[3] R. Di Taranto, S. Muppirisetty, R. Raulefs, D. Slock, T. Svensson, and H. Wymeersch, "Location-aware communications for 5G networks: How location information can improve scalability, latency, and robustness of 5G," *IEEE Signal Process. Mag.*, vol. 31, no. 6, pp. 102–112, Nov. 2014.

[4] *Study on New Services and Markets Technology Enablers; Stage 1, Release 14*, document TR 22.891, 3GPP, Jun. 2016.

[5] *Evolved Universal Terrestrial Radio Access (E-TRA); Physical Channels and Modulation, Release 9*, document TS 36.211, 3GPP, Mar. 2010.

[6] *UE Positioning in E-UTRAN—Stage 2, Release 13*, document TS 36.305, 3GPP, Jan. 2016.

[7] *Study on Indoor Positioning Enhancements for UTRA and LTE, Release 13*, document TR 37.857, 3GPP, Sep. 2015.

[8] *New SID: Study on LTE Vehicular Positioning Technologies*, document RP-162521, Intel Corp., RAN-74, Dec. 2016.

[9] J. Medbo, I. Siomina, A. Kangas, and J. Furuskog, "Propagation channel impact on LTE positioning accuracy: A study based on real measurements of observed time difference of arrival," in *Proc. IEEE PIMRC*, Sep. 2009, pp. 2213–2217.

[10] "Establishing criteria for the accuracy and reliability of the caller location information in support of emergency services," Electron. Commun. Committee, Copenhagen, Denmark, Tech. Rep. ECC 225, Oct. 2014.

[11] M. Driusso, F. Babich, F. Knutti, M. Sabathy, H. Mathis, and C. Marshall, "Vehicular position tracking using LTE signals," *IEEE Trans. Veh. Technol.*, vol. 66, no. 4, pp. 3376–3391, Apr. 2017.

[12] K. Shamaei, J. Khalife, and Z. Kassas, "Exploiting LTE signals for navigation: Theory to implementation," *IEEE Trans. Wireless Commun.*, vol. 17, no. 4, pp. 2173–2189, Apr. 2018.

[13] I. Güvenç and C.-C. Chong, "A survey on TOA based wireless localization and NLOS mitigation techniques," *IEEE Commun. Surveys Tuts.*, vol. 11, no. 3, pp. 107–124, 3rd Quart., 2009.

[14] C. Gentner, E. Muñoz, M. Khider, E. Staudinger, S. Sand, and A. Dammann, "Particle filter based positioning with 3GPP-LTE in indoor environments," in *Proc. IEEE/ION PLANS*, Apr. 2012, pp. 301–308.

[15] S. H. Kong and B. Kim, "Error analysis of the OTDOA from the resolved first arrival path in LTE," *IEEE Trans. Wireless Commun.*, vol. 15, no. 10, pp. 6598–6610, Oct. 2016.

[16] P. Müller, J. A. del Peral-Rosado, R. Piché, and G. Seco-Granados, "Statistical trilateration with skew-t distributed errors in LTE networks," *IEEE Trans. Wireless Commun.*, vol. 15, no. 10, pp. 7114–7127, Oct. 2016.

[17] D. Dardari, C.-C. Chong, and M. Z. Win, "Threshold-based time-of-arrival estimators in UWB dense multipath channels," *IEEE Trans. Commun.*, vol. 56, no. 8, pp. 1366–1378, Aug. 2008.

[18] D. Dardari, A. Conti, U. Ferner, A. Giorgetti, and M. Z. Win, "Ranging with ultrawide bandwidth signals in multipath environments," *Proc. IEEE*, vol. 97, no. 2, pp. 404–426, Feb. 2009.

[19] W. Xu, M. Huang, C. Zhu, and A. Dammann, "Maximum likelihood TOA and OTDOA estimation with first arriving path detection for 3GPP LTE system," *Trans. Emerg. Telecommun. Technol.*, vol. 27, no. 3, pp. 339–356, Nov. 2014.

[20] X. Li and K. Pahlavan, "Super-resolution TOA estimation with diversity for indoor geolocation," *IEEE Trans. Wireless Commun.*, vol. 3, no. 1, pp. 224–234, Jan. 2004.

[21] T. Wang, Y. Shen, S. Mazuelas, H. Shin, and M. Z. Win, "On OFDM ranging accuracy in multipath channels," *IEEE Syst. J.*, vol. 8, no. 1, pp. 104–114, Mar. 2014.

[22] J. A. del Peral-Rosado, J. A. López-Salcedo, G. Seco-Granados, F. Zanier, and M. Crisci, "Joint maximum likelihood time-delay estimation for LTE positioning in multipath channels," *EURASIP J. Adv. Signal Process.*, vol. 2014, no. 1, pp. 1–13, Mar. 2014.

[23] *Evolved Universal Terrestrial Radio Access (E-UTRA); User Equipment (UE) Radio Transmission and Reception, Release 13*, document TS 36.101, 3GPP, Jul. 2015.

[24] *Study on 3D Channel Model for LTE, Release 12*, document TR 36.873, 3GPP, Sep. 2014.

[25] *E-UTRA—Radio Frequency (RF) System Scenarios, Release 13*, document TR 36.942, 3GPP, Jan. 2016.

[26] F. Gustafsson and F. Gunnarsson, "Mobile positioning using wireless networks: Possibilities and fundamental limitations based on available wireless network measurements," *IEEE Signal Process. Mag.*, vol. 22, no. 4, pp. 41–53, Jul. 2005.

[27] D. B. Jourdan, D. Dardari, and M. Z. Win, "Position error bound and localization accuracy outage in dense cluttered environments," in *Proc. IEEE Int. Conf. Ultra-Wideband*, Sep. 2006, pp. 519–524.

[28] N. Liu, Z. Xu, and B. M. Sadler, "Geolocation performance with biased range measurements," *IEEE Trans. Signal Process.*, vol. 60, no. 5, pp. 2315–2329, May 2012.

[29] E. G. Larsson, G. Liu, J. Li, and G. B. Giannakis, "Joint symbol timing and channel estimation for OFDM based WLANs," *IEEE Commun. Lett.*, vol. 5, no. 8, pp. 325–327, Aug. 2001.

[30] S. Kay, *Fundamentals of Statistical Signal Processing: Estimation Theory*, vol. 1. Englewood Cliffs, NJ, USA: Prentice-Hall, 1998.

[31] M. D. Larsen, G. Seco-Granados, and A. Swindlehurst, "Pilot optimization for time-delay and channel estimation in OFDM systems," in *Proc. IEEE ICASSP*, May 2011, pp. 3564–3567.
[32] R. Montalbán, J. A. López-Salcedo, G. Seco-Granados, and A. L. Swindlehurst, "Power allocation method based on the channel statistics for combined positioning and communications OFDM systems," in *Proc. IEEE ICASSP*, May 2013, pp. 4384–4388.
[33] D. G. Manolakis, V. K. Ingle, and S. M. Kogon, *Statistical and Adaptive Signal Processing: Spectral Estimation, Signal Modeling, Adaptive Filtering and Array Processing*. Norwood, MA, USA: Artech House, 2005.
[34] J. A. del Peral-Rosado *et al.*, "Comparative results analysis on positioning with real LTE signals and low-cost hardware platforms," in *Proc. NAVITEC*, Dec. 2014, pp. 1–8.
[35] Y. Li, "Blind SNR estimation of OFDM signals," in *Proc. IEEE ICMMT*, May 2010, pp. 1792–1796.

JOSÉ A. DEL PERAL-ROSADO (S'12–M'15) received the Ph.D. degree in telecommunications engineering from the Universitat Autònoma de Barcelona (UAB) in 2014. Since 2014, he has been a Post-Doctoral Researcher with the Department of Telecommunications and Systems Engineering, UAB. From 2014 to 2016, he was a Visiting Researcher with the European Space Research and Technology Centre, European Space Agency under the NPI program. He is actively involved in COST CA15104 (IRACON), and he gave tutorials at IEEE conferences ICC'17 and PIMRC'17. His research interests are in signal processing with applications to communications and navigation based on satellite and terrestrial technologies.

JOSÉ A. LÓPEZ-SALCEDO (M'10–SM'16) received the M.Sc. and Ph.D. degrees in telecommunication engineering from the Universitat Politècnica de Catalunya, in 2001 and 2007, respectively. In 2006, he joined the Department of Telecommunications and Systems Engineering, Universitat Autònoma de Barcelona, Spain, where he is currently an Associate Professor. He has been the principal investigator of more than 10 research projects, most of them funded by the European Space Agency. He has held several visiting appointments at the Coordinated Science Laboratory, the University of Illinois Urbana-Champaign, the University of California, Irvine, and the European Commission, Joint Research Centre. His research interests lie in the field of signal processing for communications and navigation.

FRANCESCA ZANIER received the M.E. degree *(cum laude)* in telecommunications engineering and the Ph.D. degree in information engineering from the University of Pisa, Pisa, Italy, in 2004 and 2009, respectively. During the Ph.D. studies, she cooperated with the Radio Navigation Working Group, European Space Agency (ESA)/European Space Research and Technology Centre (ESTEC), Noordwijk, The Netherlands, concerning aspects on signal design for future GNSS. Since 2009, she has been a Radionavigation System Engineer with ESA/ESTEC. Her research activities are mainly focused on digital communication theory and signal processing, with special emphasis on signal design and processing for satellite positioning systems and their hybridization with terrestrial systems.

GONZALO SECO-GRANADOS (S'97–M'02–SM'08) received the Ph.D. degree in telecommunications engineering from the Universitat Politècnica de Catalunya, Spain, in 2000, and the M.B.A. degree from the IESE Business School, Spain, in 2002. From 2002 to 2005, he was a Member of the European Space Agency, involved in the design of the Galileo System. Since 2006, he has been an Associate Professor with the Department of Telecommunications and Systems Engineering, Universitat Autònoma de Barcelona, Spain, and has been serving as a Vice Dean of the Engineering School, since 2011. He has been a principal investigator of more than 25 research projects. In 2015, he was a Fulbright Visiting Professor with the University of California at Irvine, Irvine, CA, USA. His research interests include the design of signals and reception techniques for satellite and terrestrial localization systems, multi-antenna receivers, and positioning with 5G technologies. He was a recipient of the 2013 ICREA Academia Award. Since 2018, he is serving as Member of the Sensor Array and Multichannel Technical Committee of the IEEE Signal Processing Society.